Article

Structural Characterization and Binding Studies of the Ectodomain G Protein of Respiratory Syncytial Virus Reveal the Crucial Role of pH with Possible Implications in Host−Pathogen Interactions

Abu Hamza, Zoya Shafat, Zahoor Ahmad Parray, Malik Hisamuddin, Wajihul Hasan Khan, Anwar Ahmed, Fahad N. Almajhdi, Mohamed A. Farrag, Arif Ahmed Mohammed, Asimul Islam, and Shama Parveen*

Read Online

ACCESS | Metrics & More | Article Recommendations

ABSTRACT: Respiratory syncytial virus (RSV) is a leading viral pathogen causing acute lower respiratory tract infection in children. The G protein of RSV is involved in attachment with the host cell. It is a neutralizing antigen and thus a vaccine candidate. Heparan sulfate is a type of glycosaminoglycan (GAG) present on the host cell membrane that is involved in attachment with the G protein of RSV. We describe a novel approach for efficient expression and purification of the ectodomain G protein in the prokaryotic system and its biophysical characterization. The native ectodomain G protein was purified using a two-step process by Ni-NTA and DEAE weak anion-exchange chromatography through the supernatant obtained after cell lysis. In addition, the denatured form of the protein was also purified from the solubilized inclusion bodies (IBs) by Ni-NTA affinity chromatography with a higher yield. Dynamic light scattering (DLS) was performed to confirm the homogeneity of the purified protein. The effect of pH on the stability and structure of the purified protein was studied by circular dichroism (CD), fluorescence, and absorbance spectroscopy techniques. Isothermal titration calorimetry (ITC) and microscale thermophoresis (MST) were exploited to demonstrate the interaction of heparan sulfate with the ectodomain G protein. The dynamic light scattering results showed that the purified protein was homogenic and had a well-folded native conformation. Biophysical characterization of the protein revealed that it was stable and had intact secondary and tertiary structures at pH 7.5. CD analysis revealed that the protein showed a loss in the secondary structure at pH values 5.5 and 3.5, while absorbance spectroscopy suggested a stable tertiary structure at pH values 7.5 and 5.5 with a probable aggregation pattern at pH 3.5. This loss in the structure of the ectodomain G protein at low pH can be correlated with its physiological activity. A slight change in pH might play a crucial role in host−pathogen interactions. The fluorescence intensity of the protein decreased on moving toward a lower pH with no spectral shift in emission maxima. In addition, isothermal titration calorimetry and microscale thermophoresis results showed strong binding affinity of the ectodomain G protein with heparan sulfate. The binding of heparan sulfate with protein was probably due to the electrostatic interaction of positively charged amino acid residues of the heparin-binding domain of the protein and the negatively charged group of GAGs. Future studies may involve the development of possible therapeutic agents interacting with the G protein and affecting the overall charge and pH that might hinder the host−pathogen interaction.
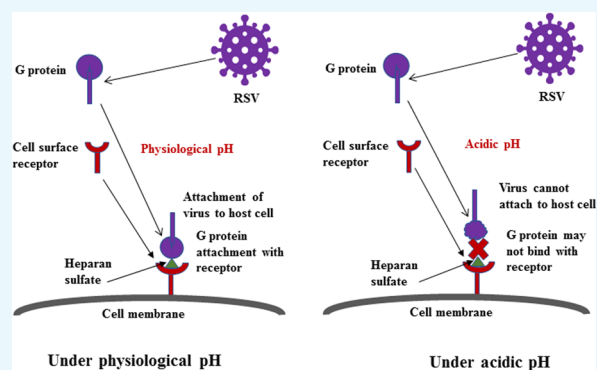
1. INTRODUCTION

Respiratory syncytial virus (RSV) leads to around 33.8 million cases across the globe and hospitalization of 2.8−4.3 million individuals with 66 000−99 000 deaths annually, and most of the deaths occur in children below 5 years.[1,2] RSV belongs to the genus *Orthopneumovirus* and family Pneumoviridae.[3] RSV is an enveloped virus, and its genome is negative-sense, nonsegmented, single-stranded RNA of approximately 15.2 kb in length that encodes for 11 proteins. The nucleocapsid of the RSV is bounded by a lipid envelope where three trans-
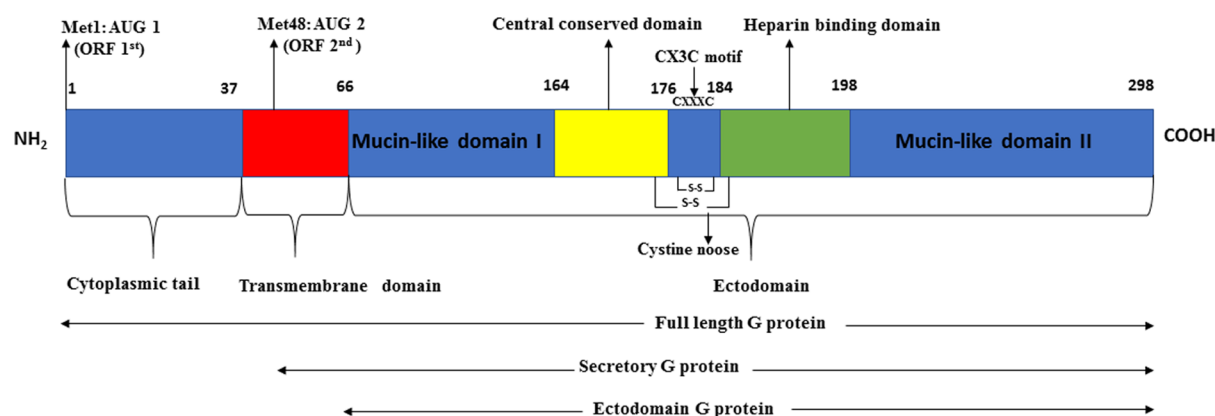
membrane glycoproteins SH, F, and G are embedded that play an important role in viral entry, fusion and attachment, respectively. The G protein of RSV is a type II transmembrane

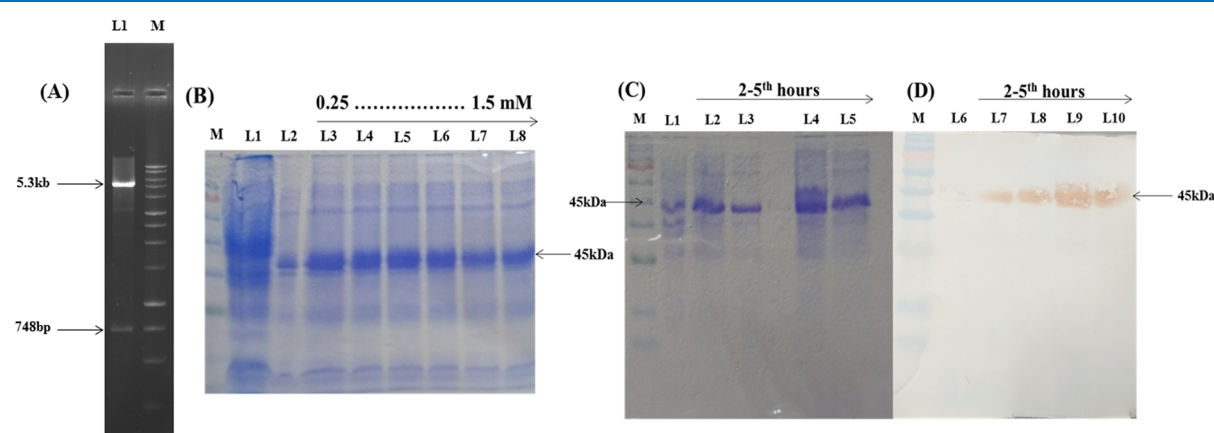**Figure 1.** Schematic representation of G glycoprotein showing different regions that include the cytoplasmic tail, transmembrane domain, and ectodomain. The ectodomain contains a central conserved domain (CCD), cysteine noose (Cys noose), CX3C motif, and heparin-binding domain (HBD). The soluble G protein was produced through another initiation site, Met48.


Figure 2. (A) Restriction digestion products of the recombinant pET-28a vector. Lane 1: released insert [ectodomain G protein gene (748 bp)]; Lane M: molecular weight marker. (B) SDS-PAGE gel photograph showing the expression of ectodomain G protein (45 kDa) induced by increasing the concentration of IPTG at 37 °C. Lane M: molecular mass marker; Lane 1: vector without insert; Lane 2: un-nduced bacterial pellet; and Lanes 3−8: pellet induced with 0.25, 0.5, 0.75, 1.0, 1.25, and 1.50 mM IPTG, respectively. (C) SDS-PAGE gel photograph showing the expression of ectodomain G protein induced with 0.5 mM IPTG at 37 °C. Lane 1: uninduced pellet; Lanes 2−5: induced pellet after the 2nd to 5th h, respectively. (D) Western blot showing the expression of ectodomain G protein at different hours after induction with 0.5 mM IPTG at 37 °C. Lane 6: uninduced pellet; Lanes 7−10: induced pellet after the 2nd to 5th h, respectively; and Lane M: molecular mass marker.

glycoprotein, which helps in virion attachment to the host cell. It acts as a neutralizing antigen and hence is a good candidate for vaccine development.[4] The length of G protein may vary from 282 to 321 amino acids.[5] The G protein of RSV consists of three main domains (Figure 1), namely, the cytoplasmic domain (residues 1−37), transmembrane/anchor domain (residues 38−66), and ectodomain (residues 67−298).[6] The C-terminal region of the ectodomain G protein contains two hypervariable segments, which are accountable for the variability.[7] The ectodomain G protein has a stretch of a centrally conserved 13 amino acid region (164−176aa), which is highly conserved, among all RSV strains.[8,9] This region has a cluster of four cysteine residues (173, 176, 182, and 186) that are held together by two disulfide bonds (between Cys173−Cys186 and Cys176−Cys182) with the residues spanning the third cysteine (Cys182) and fourth cysteine (Cys186) forming a CX3C motif. This region forms a cystine nooselike motif, which facilitates the attachment of RSV to human airway epithelial (HAE) cells by interaction with CX3CR1 during natural infection.[10,11] Immediately downstream of the cystine noose lies the glycosaminoglycan (GAG)/heparin binding region (HBR) from 184 to 198, encompassing a residue of

positively charged amino acids, which facilitated the attachment to heparan sulfate and other glycosaminoglycans.[12] GAGs are long, linear, unbranched polymers of replicating disaccharide units that form proteoglycans in the extracellular matrix and are covalently bound to the host cell membrane protein. Generally, GAGs are highly sulfated and have a negative charge. A recent study indicated that the HBR in the G protein mediates attachment of RSV to negatively charged heparan sulfate via basic amino acids.[12,13] Previously, it was shown that heparan sulfate and to some extent chondritin-4-sulfate had been involved in virion attachment with the host cell membrane.[14]

The G protein gene of RSV has been extensively used for phylogenetic analysis.[15−17] Some of the investigations have attempted cloning and expression of the RSV G gene in the bacterial system for antigenic characterization.[18,19] Although information is available about the function of the G protein, limited data is available that demonstrates its structural properties. The structural characterization of G protein and its role in viral infection under physiological conditions need to be investigated in detail. The ectodomain G-protein-encoding gene has been cloned, expressed, and purified at suboptimal
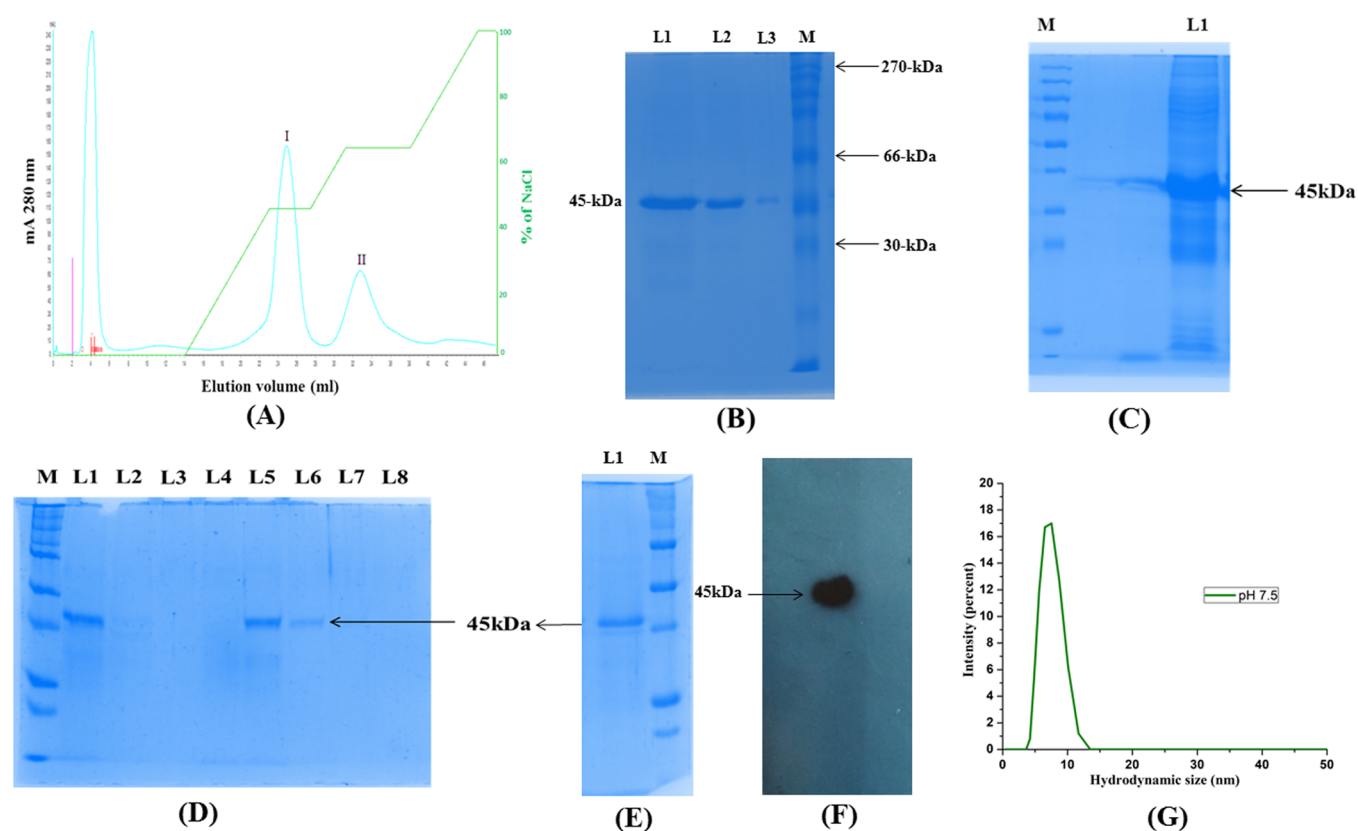
Figure 3. Purification of the ectodomain G protein. (A) Elution profile at 280 nm (milli absorbance) versus elution volume (mL) of the weak anion exchanger (HiTrap DEAE FF). The second (light green) curve indicates the gradient of sodium chloride (0−100%) where buffer A has 10 mM Tris buffer of pH 8.0 and buffer B has 1.0 M sodium chloride. (B) SDS-PAGE of the purified native ectodomain G protein. Lanes 1 and 2: peak I of the chromatogram (HiTrap DEAE FF) showing the purified ectodomain G protein containing 150 and 100 μg of protein; lane 3: peak II; and Lane M: molecular mass marker. (C) SDS-PAGE gel photograph showing the inclusion bodies (IBs) of the ectodomain G protein (Lane 1). (D) SDS-PAGE showing the elution profile of Ni-NTA column chromatography. Lane 1: supernatant; lane 2: flow throw; lane 3: washing; and lanes 4−8: elution with 50, 100, 150, 300, and 500 mM imidazole, respectively. (E) SDS-PAGE of the purified ectodomain G protein. Lane 1: purified ectodomain G protein (45 kDa). (F) Western blot of the purified ectodomain G protein. (G) Dynamic light scattering profile of the purified ectodomain G protein. (The *X*-axis shows the radius (nm), and the *Y*-axis represents the intensity (%)).

levels by our research group in a previous study.[20] In this study, the ectodomain G protein showed expression in the inclusion bodies (IBs). We solubilized the IBs using 8 M urea followed by its purification using affinity chromatography. However, the protein showed minimal expression with a negligible amount of protein in the soluble form. Therefore, in the present study, we have continued modification of the expression and purification protocols. We used the same clone of the ectodomain G protein and have optimized the conditions for the purification of the protein under native conditions from the supernatant in a soluble form as well as from the solubilized IBs in a denatured form. The effect of pH on tertiary and secondary structures of the ectodomain G protein was evaluated by absorbance, fluorescence, and circular dichroism spectroscopy techniques. In addition, the binding studies of the ectodomain G protein with heparan sulfate were carried out by isothermal titration calorimetry (ITC) and microscale thermophoresis (MST). It was interesting to determine the possible capacity of binding of the ectodomain G protein with the host cell and estimate the importance of GAGs in host−viral interactions. Moreover, structural characterization and binding studies of G protein may also facilitate the process of drug designing and vaccine development, which might assist in preventing the RSV infection.

2. RESULTS

2.1. Expression of Ectodomain G Protein. The recombinant pET-28a vector harboring the ectodomain G protein gene was transformed into BL21 (DE3) competent cells of *Escherichia coli*, and the isolated plasmid was confirmed by agarose gel electrophoresis with double digestion using *Bam*H1 and *Sal* 1 endonucleases (Figure 2A). The cells were grown in Luria−Bertani (LB) medium with different isopropyl-1-thio-β-D-galactopyranoside (IPTG) concentrations used for optimum expression of the recombinant ectodomain G protein at 37 °C. No significant change was observed in the expression of protein beyond the 0.5 mM IPTG concentration (Figure 2B). Therefore, the 0.5 mM IPTG concentration was considered for optimization studies. The expression of ectodomain G proteins was also checked with 0.5 mM IPTG induction up to a post-induction period of 5 h at 37 °C. The cells were collected at every 1 h interval, and the cell lysate was analyzed by sodium dodecyl sulfate-polyacrylamide gel electrophoresis (SDS-PAGE) and Western blotting. The ectodomain G protein showed maximal expression after a 4 h post-induction period (Figure 2C,D).

2.2. Purification of the Ectodomain G Protein in Native Conditions. The soluble ectodomain G protein was purified from the bacterial cell extract after lysis and sonication followed by centrifugation. The protein present in the
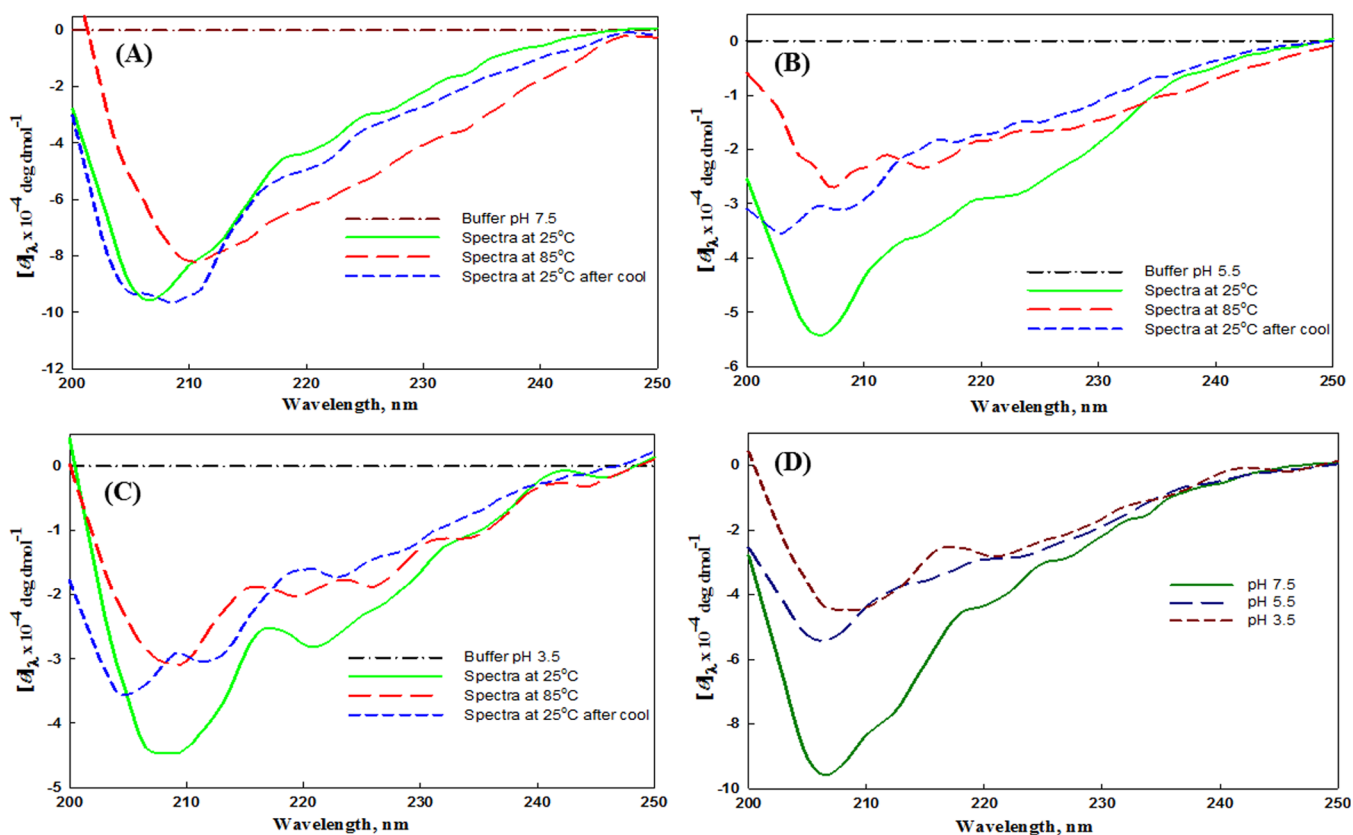
Figure 4. Far-UV CD spectra of the ectodomain G protein. Green, red, and blue represent spectra at 25, 85, and 25 °C after cooling, respectively. CD spectra of the ectodomain G protein (A) at pH 7.5, (B) at pH 5.5, and (C) at pH 3.5. (D) CD spectra of the ectodomain G protein at pH 7.5 (dark green), pH 5.5 (dark blue), and pH 3.5 (dark red). The spectrum at pH 7.5 is considered as control.

supernatant was purified under the native conditions at 4 °C. However, a little amount of ectodomain G protein was present in a soluble form because a major fraction of the protein was expressed in inclusion bodies (IBs). Thereafter, we proceeded for the ectodomain G protein purification using both native (supernatant) and denatured (IBs) conditions. The native ectodomain G protein was purified to homogeneity by Ni-NTA affinity and DEAE ion-exchange chromatography using two different chromatographic steps. The ectodomain G protein purified after Ni-NTA chromatography showed some nonspecific bands of bacterial proteins. Hence, the eluted protein was dialyzed extensively, concentrated, and subjected to DEAE anion-exchanger column chromatography to obtain its pure form. The protein bound to the column was eluted with a linear gradient of NaCl (1 M NaCl 0−100%). Three peaks along with an unbound fraction (highest peak) were collected. The first and second peaks were eluted at a 0.45 and 0.64 M ionic strength of NaCl, respectively (Figure 3A). The protein eluted at 0.45 M NaCl clearly showed a 45 kDa single band on SDS-PAGE, indicating its purity (Figure 3B). After anion-exchange chromatography, we were able to recover 0.35 mg mL^{-1} protein.
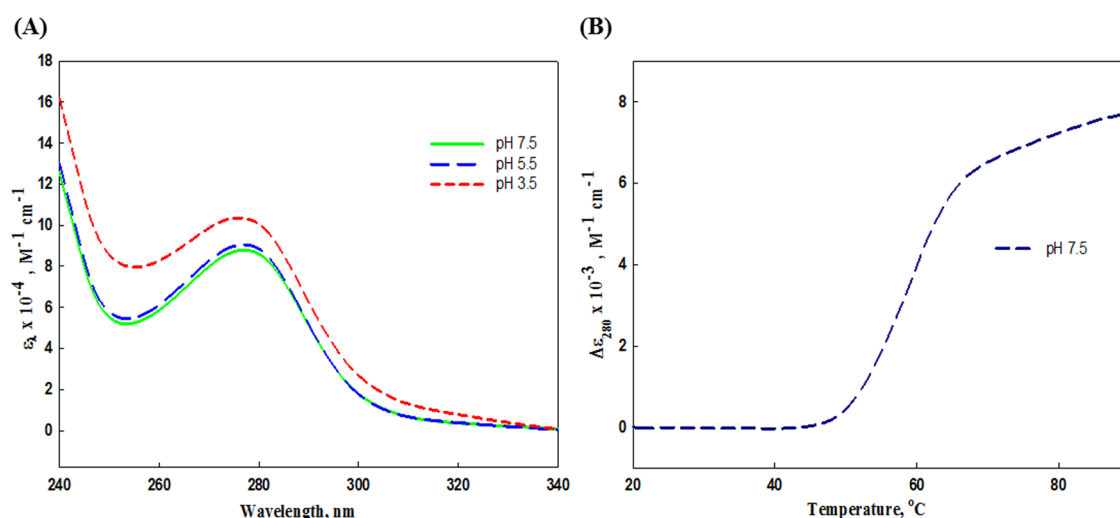
2.3. Purification of the Ectodomain G Protein from Inclusion Bodies. The ectodomain G protein was also purified under denatured conditions. Purified IBs were isolated from bacterial cell extracts by washing with lysis buffer and Milli-Q water to eliminate contamination of proteases, host protein, DNA, endotoxins, and nonspecific proteins.[21] Purified IBs showed an intense band at 45 kDa on SDS-PAGE (Figure 3C). Isolated IBs were solubilized in *N*-lauroylsarcosine and

purified by Ni-NTA affinity chromatography in a single step with increasing concentrations of imidazole (50−500 mM). SDS-PAGE showed that the desired ectodomain G protein was eluted at 100 and 200 mM imidazole (Figure 3D).

2.4. Protein Refolding. Protein refolding is the crucial step to get rid of denaturants and thus provides a better environment for proteins to refold into their native conformations spontaneously. The purified proteins were gradually dialyzed against 25 mM Tris buffer, pH 7.5, having 5% glycerol, 100 mM NaCl, and 1 mM redox shuffling agent (reduced and oxidized glutathione), for 24 h at 4 °C to obtain the refolded protein. Subsequently, the protein was centrifuged and passed through a 0.22 μm membrane filter to get rid of protein precipitates, which could have formed during the refolding process. SDS-PAGE and Western blot indicated a single purified band of the ectodomain G protein (Figure 3E,F).

2.5. Dynamic Light Scattering. Dynamic light scattering (DLS) measurements were performed to confirm the homogeneity and hydrodynamic size (d_H) of the purified ectodomain G protein. This technique has been performed to recognize the folding, unfolding, and aggregation behaviors of the proteins.[22] The d_H value of the purified ectodomain G protein was found to be 7.4 nm (Figure 3G).

2.6. Analysis of Spectral Measurement. The secondary structure and backbone orientation of the purified protein were monitored with different pH values using far-UV circular dichroism (CD) (200−250 nm) at 25 °C. The far-UV CD spectrum of the ectodomain G protein at physiological pH 7.5 suggested that the structure of the protein is a mixture of *β*-

(A)

(B)

Figure 5. (A) Absorbance spectra of the ectodomain G protein at pH 7.5 (green), pH 5.5 (blue), and pH 3.5 (red). Absorbance spectra of the sample were measured from 340 to 240 nm as a function of pH at 25 °C. The spectrum at pH 7.5 is considered as control. (B) Representative curve of thermal denaturation of the ectodomain G protein monitored at 280 nm and pH 7.5. Denaturation curves were recorded in the temperature range of 20−90 °C.

sheet and α-helix with two ellipticity minima at 208 and 222 nm.[23] We recorded the far-UV CD spectra at 25 and 85 °C and then again at 25 °C after cooling to check the reversible nature of the protein. We also observed the behavior of the protein's secondary structure content at different pH values. The ectodomain G protein was stable and reversible at pH 7.5 (Figure 4A), while it was irreversible after cooling at pH values 5.5 and 3.5 (Figure 4B,C). Interestingly, we found a significant decrease in the intensity of far-UV spectra on moving from pH 7.5 to 3.5 at 25 °C (Figure 4D). The spectra of ectodomain G protein suggested that it has its secondary structure content at pH 7.5. In contrast, on moving toward acidic pH (5.5 and 3.5), the intensity of far-UV spectra decreased and there was a loss of secondary structure content. Taken together, our observation suggested that the ectodomain G protein maintains its secondary structure at physiological pH, whereas it loses most of the secondary structure at acidic pH values.

We also performed absorbance spectroscopy at 25 °C from 240 to 340 nm to estimate the tertiary structure of the protein. The spectra were observed at three different pH values: 7.5, 5.5, and 3.5. The tertiary structure was almost similar at pH 7.5 and 5.5. In contrast, an increase in absorption spectra was noticed without any shifting of absorption maxima at pH 3.5, suggesting that at this pH the protein is losing the tertiary structure. In addition, due to the aggregation at pH 3.5, some of the scatterings were also observed at 320−340 nm (Figure 5A).

2.7. Analysis of Thermal Denaturation Curves. To observe the effect of heat, we have studied the thermal denaturation of the ectodomain G protein at 280 nm and pH 7.5. To measure thermodynamic parameters like melting temperature (T_m) and change in enthalpy (ΔH_m) of the protein, we heated the protein sample from 20 to 90 °C. The thermal denaturation curve was analyzed to obtain the values of T_m and ΔH_m. The T_m and ΔH_m were found to be 56.95 °C and 57.07 ($\pm$1.2), respectively (Figure 5B).

2.8. Fluorescence Measurements. Fluorescence spectral studies give information about the tertiary structure of the protein. The intrinsic fluorescence measurements of a protein are due to the aromatic amino acid residue, which is very

sensitive to its local milieu. The ectodomain G protein has two tyrosine (Tyr) and one tryptophan (Trp) residues that allowed us to perform the intrinsic fluorescence measurements to observe the effect of pH on the protein's tertiary structure and observe the structural changes of aromatic amino acids. We monitored the emission spectra in the region of 300−400 nm, and the excitation wavelength of the protein was set at 280 nm. The change in intrinsic fluorescence of the ectodomain G protein at three different pH values (pH 7.5, 5.5, and 3.5) is shown in Figure 6.
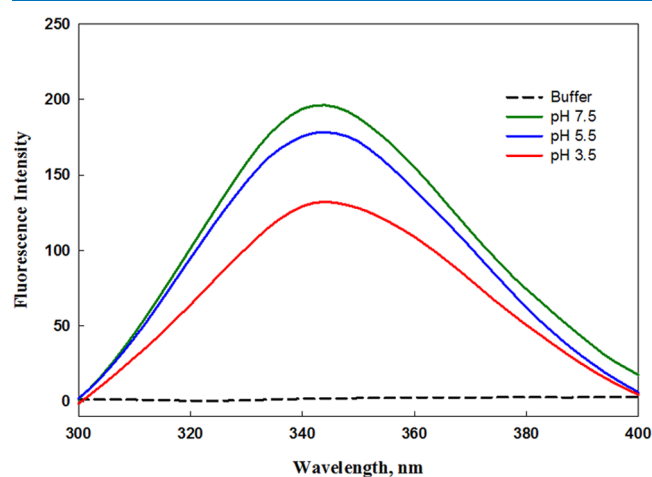
Figure 6. Fluorescence spectra of the ectodomain G protein at three different pH values. The protein sample was excited at 280 nm, and the emission spectra were recorded from 300 to 400 nm at 25 °C.

2.9. Isothermal Titration Calorimetry. The thermodynamic binding parameters of the ectodomain G protein with heparan sulfate were evaluated to analyze the binding affinity measurements using ITC. Figure 7A indicates the titration of heparan sulfate against the reaction cell containing the ectodomain G protein. The upper panel of Figure 7A shows the thermogram of raw data in power versus time, and every peak in the binding isotherm signifies a single injection of ligand, while the lower panel represents the amount of heat
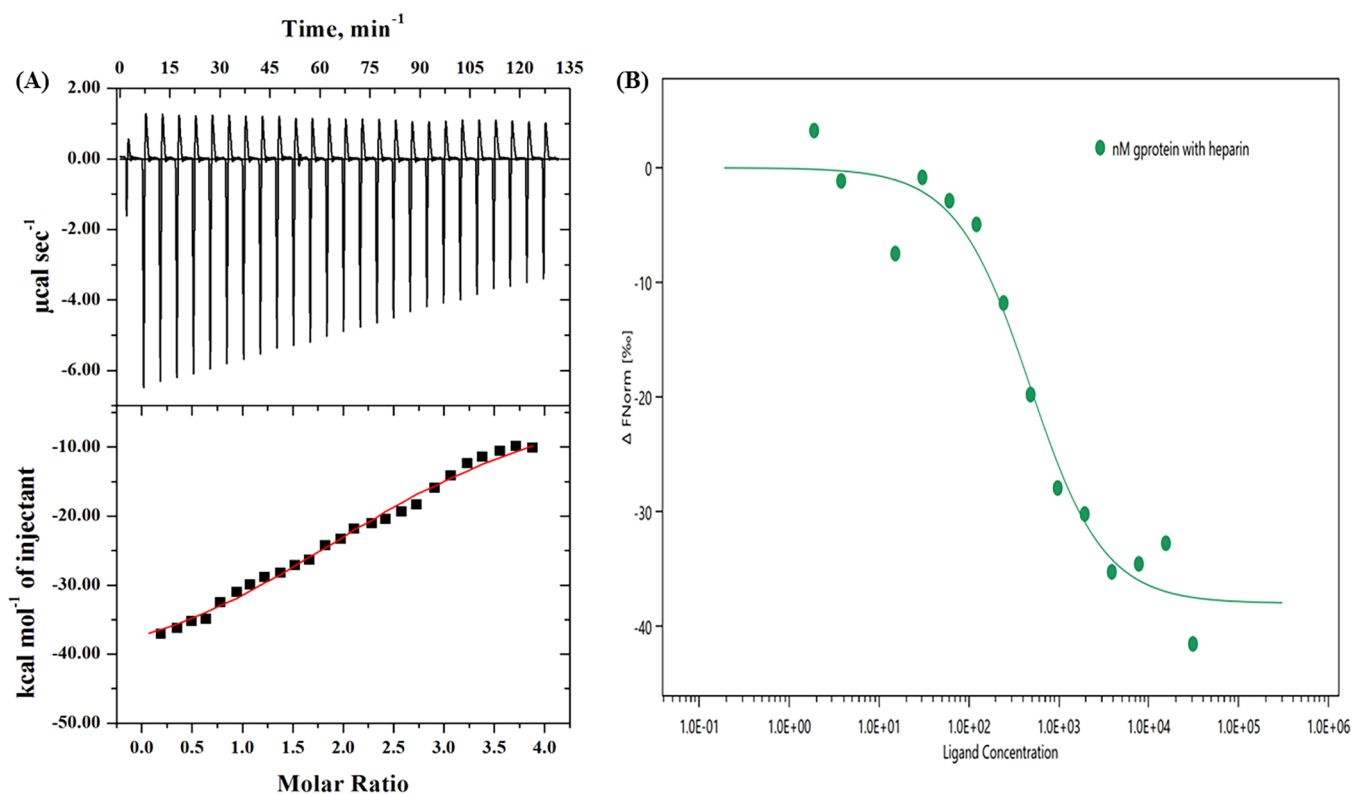
Figure 7. (A) Isothermal titration calorimetry thermograms of the ectodomain G protein (10 μM) with heparan sulfate (200 μM). The calorimetric response with a consecutive injection of heparan sulfate added to the reaction cell (upper panel) and the resulting binding isotherm (lower panel) are shown at pH 7.5 and 25 °C. (B) Microscale thermophoresis binding curve of the fluorescently labeled ectodomain G protein with heparan sulfate at physiological pH 7.5 and 25 °C.

Table 1. Thermodynamic Binding Parameters of the Ectodomain G Protein with Heparan Sulfate Evaluated from ITC at pH 7.5 and 298 K (25 °C)

thermodynamic binding parameters (units)	K_a (M^{-1})	$\Delta H°$ (cal mol^{-1})	$\Delta S°$ (cal mol^{-1} deg^{-1})	$\Delta G°$ (cal mol^{-1})
step 1	10.7×10^4 ($\pm 2.52 \times 10^3$)	-4.62×10^4 ($\pm 3.19 \times 10^3$)	-132	-6.84×10^3

released as a function of the mole ratio of the ligand to the protein. The origin software (VP-ITC) was used to fit the profiles of heat change. The parameters like binding enthalpy ($\Delta H°$), association constant (K_a), and change in entropy ($\Delta S°$) were used to calculate the Gibbs free-energy change ($\Delta G°$) using eq 2. The values of thermodynamic binding parameters of these bimolecular reactions at pH 7.5 and 298 K (25 °C) are given in Table 1.

2.10. Microscale Thermophoresis (MST) Analysis. MST experiments were performed with a constant concentration of the NHS-labeled ectodomain G protein, whereas the concentration of the nonlabeled heparan sulfate was varied. Protein samples were loaded using MST standard capillaries and analyzed using Monolith NT.115. A K_d value of 426 nM was obtained with a signal-to-noise ratio of 13.3. The MST analysis showed a strong binding affinity of heparan sulfate with the ectodomain G protein as shown in Figure 7B.

3. DISCUSSION

In the pediatric age group, RSV is the most common viral pathogen of respiratory tract disease. The RSV G protein plays a significant role in inducing and modulating the host immune response against infection.[24] RSV infection induces neutralizing antibodies against the G proteins, which thus act as vaccine candidates.[4,25] The interaction between the G protein and the CX3CR1 receptor is involved in immune response modulation, which leads to infection aggravation in the host cell. Hence, the G protein is proficient to suppress the process of inflammation, adaptive and innate immune responses, and production of β-interferon and T-lymphocytes.[26−28] A recent study demonstrated that antibodies raised against the G protein of RSV preserved the nonglycosylated region, indicating that they could be used as a prophylactic treatment to prevent RSV infection. The *in vivo* study also revealed that these antibodies promote a reduction in the infection and viral titer.[29,30] Recently, Fuentes and colleagues showed that the nonglycosylated G protein produced by bacteria could be used as a safe and effective vaccine against RSV infection.[31] Another recent study has shown the interaction of flavonoids (quercetin and morin) with the bacterium-expressed ectodomain G protein by fluorescent quenching.[32] Previous studies have reported limited information on cloning and expression of the G protein of RSV.[18,19,33] Hence, the present study focuses on the production of the ectodomain G protein in large quantity in a bacterial system and its secondary and tertiary structure characterization by CD, fluorescence, and absorbance spectroscopy techniques. The binding studies of the ectodomain G protein with heparan sulfate were also carried out by isothermal titration calorimetry and microscale thermophoresis.

Different parameters were optimized for maximal protein expression including inducer concentration, temperature, and post-induction time interval. Maximal ectodomain G protein was expressed at 0.5 mM IPTG in BL21 (DE3) after 4 h of post-induction period. The expression at 16 °C indicates that a considerable amount of the protein was present in the supernatant as compared to the expression at 37 °C. Therefore, to obtain the protein in the native condition, the expression was carried out at 16 °C, whereas to obtain a large amount of protein, which was aggregated to form inclusion bodies, was processed at 37 °C.

Initially, the protein was purified under native conditions using two different steps, Ni-NTA and DEAE ion-exchange chromatography. Protein obtained after Ni-NTA affinity chromatography showed some undesirable bands. Thus, the eluted fraction was further subjected to DEAE ion-exchange chromatography to obtain a pure protein. The yield of the ectodomain G protein purified under native conditions was quite low; however, the major portion of the protein aggregated to form inclusion bodies (IBs). Inclusion bodies may be formed due to inappropriate folding of the eukaryotic membrane protein in the prokaryotic system that leads to their misfolding and mistargeting.[34−36] Optimization of protein expression, IB solubilization, and refolding of the denatured protein are the crucial steps to obtain proteins in their native form. To solubilize the IBs, 1% N-lauroylsarcosine was used because it seems to allow refolding of the solubilized protein with less aggregation than that seen with other denaturants. The IBs were completely solubilized and purified with a relatively simple purification method. We effectively solubilized the IBs in 1% N-lauroylsarcosine and purified the protein by Ni-NTA affinity chromatography using a single-step purification method. The protein was refolded into a biologically active form through dialysis, and the yield was about 20 mg L^{-1}. The protein isolated from the IBs had a similar structure to the protein obtained from the soluble supernatant. Hence, we got the refolded protein even from the IBs with higher yields. Dynamic light scattering (DLS) confirmed the homogeneity of the purified ectodomain G protein. The DLS analysis revealed a single peak with a hydrodynamic size of 7.4 nm, suggesting a well-folded protein in the native conformation.

The attachment of virion to the host cell is arbitrated by the G protein followed by fusion with the cell membrane, which is assisted by the fusion protein. This fusion may be mediated by pH-dependent pathways.[37] To observe the effect of different pH values on the stability and structure of the ectodomain G protein, we performed far-UV CD, fluorescence, and absorbance spectroscopy techniques at different pH values. Far-UV CD spectroscopy is an excellent method to determine the secondary structural content and conformation of protein as it provides information about the peptide backbone. Furthermore, the study of refolding was carried out by CD measurements with varied values of pH (3.5, 5.5, and 7.5). The spectra of our protein at different pH values were similar to that of a chymotrypsin-like fold that has a mixture of β-sheet and α-helical structures and exhibits two ellipticity minima at 222 nm and 208.[23] The ectodomain G protein spectrum at pH 7.5 was initially measured at 25 °C. The protein was then heated up to 85 °C, and the spectrum was recorded. The protein was subsequently cooled down to 25 °C, and the spectrum was remeasured. Comparison analysis of all three spectra suggested that the ectodomain G protein showed a

substantial gain in the secondary structure after heating. This indicates the reversible nature of heat-induced denaturation of the protein at pH 7.5. Similarly, the reversibility measurements of the protein were also done at pH values 3.5 and 5.5, which were not as significant as those at pH 7.5. The renaturation studies of the ectodomain G protein showed that the denatured protein failed to refold back at acidic pH (pH 3.5 and 5.5), whereas it regained its secondary structure at physiological pH (7.5). The CD data also suggested that the protein was stable at pH 7.5, while it lost its major secondary structure at pH values 5.5 and 3.5 at 25 °C. The absorbance spectra of the protein were also analyzed at different pH values (3.5, 5.5, and 7.5) at 25 °C to analyze its tertiary structure. This analysis suggested that the tertiary structure of the protein was nearly similar at pH values 7.5 and 5.5, which is indicative of intact native forms at these two pH values. However, the absorbance values of the protein at pH 3.5 increased, indicating the acid-induced loss of the tertiary structure. Thus, the present spectral studies revealed that the ectodomain G protein is stable at physiological pH, while it starts losing its structure on moving toward acidic pH. Therefore, loss of structure of the ectodomain G protein at acidic pH may be correlated with its biological activity. These experiments also suggested that the possible mechanism of attachment of the ectodomain G protein at physiological conditions is pH-specific. Thus, a slight variation in the pH may lead to inhibition of the attachment and fusion of the virion that may prevent the viral entry and thus infection.

The fluorescence emission spectra of the protein at pH 7.5, which is the native condition of the protein, show an emission maximum peak at 344 nm. No spectral shift was observed in emission maxima on moving toward lower pH values (5.5 and 3.5). This analysis revealed that the microenvironment was not significantly disturbed around the aromatic amino acid residues at low pH. However, a considerable decrease in fluorescence intensity was observed on moving toward the acidic pH values. The decrease in fluorescence intensity was observed at low pH, as the buried tryptophan exposed to the polar environment, resulting in the alteration of structural properties of the protein. The decrease in fluorescence emission at low pH values was also due to the quenching mechanism. The quenching occurred due to the protonation of acidic amino acids or water molecules that are in close proximity to tryptophan residues.

Heparan sulfate is the GAG present on the host cell surface, which is involved in the attachment with the G protein of RSV. To study the binding affinity of heparan sulfate with the ectodomain G protein, isothermal titration calorimetry and microscale thermophoresis analysis were carried out. ITC provides direct information regarding the interaction of the protein with the ligand.[38,39] The information obtained from ITC may help to explain the mechanism of binding of the virion with the host cell membrane. A one-site binding model was used to analyze the ITC thermogram data (at pH 7.5 and 298 K), which provided the best fit. Each peak in the binding isotherm in Figure 7A represents the single injection of the ligand (heparin), while the lower panel represents the integration of the area under each injection peak of the heat profile that helps in generating a differential curve. The heat profile of ITC at physiological pH (7.5) is largely exothermic having a negative heat pulse, which showed a strong binding pattern between the protein and heparan sulfate (Figure 7A and Table 1). The negative value of change in enthalpy ($\Delta H°$)

= -4.62×10^4 cal mol^{-1} and Gibbs free-energy change ($\Delta G°$) = -6.84×10^3 cal mol^{-1} at pH 7.5 suggested that the reaction was spontaneous. The negative value of $\Delta G°$ and $\Delta H°$ suggested that the binding of the ligand with the protein at this pH was largely driven by the electrostatic interaction. Moreover, the negative value of the change in entropy ($\Delta S°$) showed that the bimolecular reaction was ordered at this pH. The microscale thermophoresis also showed strong binding between the protein and heparan sulfate with a K_d value of 426 nM. A previous study had demonstrated that exothermic binding interactions occurred due to the interaction of the carboxyl or negatively charged sulfate group of the heparins with the positively charged amino acid residues of the protein.[40] In the present study, the positively charged amino acid residues in the heparin-binding domain of the ectodomain G protein bind with a negatively charged group of GAGs, that is, heparan sulfate, through electrostatic interactions, which results in the formation of the protein−GAG complex. A previous study has similarly shown that the positively charged amino acids in the heparin-binding region of the G protein probably interact with heparan sulfate having a negatively charge present on the host cells.[12] It has been reported that the binding of the G protein with host cells is mainly mediated by cellular proteoglycans containing heparan sulfate, which helps in the attachment. However, the study also reported that G protein did not show binding with a mutant cell line lacking heparan sulfate.[14] Another study had shown the binding of the viral G protein of human metapneumovirus with heparin using the heparin affinity chromatography technique.[41] However, this is the first report showing the strong binding affinity of heparan sulfate with the ectodomain G protein of RSV by isothermal titration calorimetry and microscale thermophoresis.

Any therapeutic attempt to inhibit the interaction of the virus with the host cell may exploit this crucial information. The inhibitory molecules may be designed and synthesized that upon binding to the ectodomain G protein might affect its overall charge and pH, thus preventing the interaction of the ectodomain G protein with the host cell membrane. Hence, to make an effective RSV vaccine or therapeutic agent, we should understand the molecular mechanism of RSV attachment and fusion. Thus, the investigation of different viral and host cell factors using cell culture and structural biology approaches will provide a comprehensive overview of their possible role in RSV pathogenesis. Further, structural studies of ectodomain G protein intermediates at different pH values will also expand our understanding of RSV attachment and the identification of new targets.

4. CONCLUSIONS

We optimized the conditions for maximum expression of the ectodomain G protein of RSV in the bacterial system. The purification of protein was carried out using both the supernatant and IBs. Our study provides preliminary insight into the structural characteristics of the ectodomain G protein that is sensitive to pH and charges. These factors might play an essential role in the investigation of host−pathogen interactions. Exploration of the interaction of the ectodomain G protein with the inhibitory molecules based on these findings may obstruct the efficient host−pathogen interaction. Therefore, this data might be utilized toward the formulation of possible therapeutic agents against RSV. This information can also provide a baseline for the investigation of specific

mutations in the protein that might play a pivotal role in attachment and other aspects of the viral life cycle. Thus, structural determination and binding studies of the ectodomain G protein will be a step toward vaccine development, drug designing, and prevention of viral infection.

5. MATERIALS AND METHODS

5.1. Materials. Luria−Bertani (LB) broth, Luria agar, and kanamycin were purchased from Himedia, India. Sodium chloride, imidazole, boric acid, Tris−HCl buffer, EDTA, ethanol, and the Amicon Ultra 10K device were purchased from Merck (Darmstadt, Germany). Heparan sulfate, sodium dodecyl sulfate, Triton X-100, and 3,30-diaminobenzidine (DAB) were bought from Sigma, Saint Louis. All other chemicals used during the experiments were of molecular biology grade.

5.2. Reviving the Clone of the Ectodomain G Protein. The details of cloning of the ectodomain G protein gene have been described in detail by Khan et.al.[20] Briefly, the full-length G protein gene was codon-optimized (accession No. KJ690590) and inserted in the pUC57 vector using commercial services. The ectodomain of the G protein gene (748 bp gene coding for 67−298 amino acids) was amplified from this recombinant vector and was subcloned into the pET-28a expression vector. This recombinant pET-28a with the ectodomain G protein gene was revived and was used for the present study. The recombinant expression vector (pET-28a) with the ectodomain G protein gene insert was transformed into the DH5α strain. The plasmid was isolated from the bacterial cell pellet using a commercial plasmid isolation kit as per the manufacturer's instruction and confirmed by agarose gel electrophoresis.

5.3. Expression of the Ectodomain G Protein. The expression vector containing the ectodomain G protein gene was transformed into the competent cell of the BL21 (DE3) strain. Transformed bacterial cells were grown in LB medium with 50 μg mL^{-1} kanamycin for 2 h at 37 °C and 180 rpm until the optical density reached 0.6 at 600 nm. Then, 1 mL of the uninduced sample was collected, and remaining cultures were induced with 0.25, 0.50, 0.75, 1.0, 1.25, and 1.5 mM isopropyl-1-thio-β-D-galactopyranoside (IPTG) and incubated for 5 h at 37 °C for confirmation of expression at a small level. From each induced culture, 1 mL of the sample was collected and analyzed by sodium dodecyl sulfate-polyacrylamide gel electrophoresis (SDS-PAGE) along with the uninduced culture to confirm the expression of the protein. The large-scale expression was carried out by inducing with 0.5 mM IPTG and incubating at 16 °C for 18 h and 37 °C for 5 h. The bacterial cultures were harvested at 4 °C for 10 min at 6000 rpm.

5.4. Purification of the Ectodomain G Protein in Native (Supernatant) Conditions. The harvested bacterial pellets were dissolved in lysis buffer: 250 mM NaCl, 50 mM Tris buffer pH 8.0, 1 mM 1,4-dithiothretol (DTT), 1.5 mM phenyl methane sulfonyl fluoride (PMSF), 1% (v/v) Triton X-100, 0.5 mg mL^{-1} lysozyme, and 5% (v/v) glycerol. Usually, 5 mL of lysis buffer is used for 100 mL of bacterial culture. Bacterial cell lysates were sonicated and centrifuged at 4 °C for 30 min and at 12 000 rpm, and the supernatant was collected for purification. The supernatant was loaded to the Ni-NTA purification column, which was equilibrated with buffer A: 50 mM Tris buffer pH 8.0, 1 mM DTT, 250 mM NaCl, and 5% (v/v) glycerol. The undesired protein impurities were washed

with buffer A having 10 and 20 mM imidazole. The bound protein was eluted with 100−150 mM imidazole in buffer A. Eluted fractions were subjected to dialysis against 100 mM NaCl and 25 mM Tris buffer pH 7.5, and the protein was concentrated with the Amicon Ultra 10K device. After dialysis, the protein was filtered with a 0.22 μm syringe filter and further loaded on a HiTrap DEAE FF (1 mL, 7 mm × 25 mm) column that was pre-equilibrated with 50 mM Tris buffer pH 8.0, which was linked to the Akta purifier (GE Healthcare). An aliquot of 2 mL of protein was loaded into the ion-exchange column having 2 mL loop at a constant flow rate of 0.5 mL min^{-1}. The chromatography column was washed with 50 mM Tris buffer pH 8.0 to remove the unbound protein until the A_{280} reached zero. The bound protein was eluted from the chromatography column with a linear gradient of NaCl (0−1 M NaCl w/v). The topmost peak of the eluted fraction was analyzed by SDS-PAGE to confirm the purity of the protein.

5.5. Purification of the Ectodomain G Protein from Inclusion Bodies. We purified the protein in the native condition in a soluble form, but its yield was extremely low. Thus, we used another method for purification of protein because a significantly high expression was observed in IBs. Centrifuged *E. coli* cell pellets were dissolved in the buffer (100 mM NaCl, 50 mM Tris−HCl (pH 8.0), 20 mM EDTA, 1.5 mM PMSF, and 1% Triton X-100) and lysed with sonication and centrifugation at 10 000 rpm for 40 min at 4 °C. Again, the pellet was washed off 3−4 times with autoclaved Milli-Q water through centrifugation to remove any impurities. Finally, IBs were dissolved in 5 mL of Milli-Q water. For purification, IBs were solubilized in buffer B, which has 100 mM NaCl and 50 mM Tris buffer pH 8.0 having 1% (w/v) *N*-lauroylsarcosine, for 3−4 h at 25 °C followed by centrifugation at 10 000 rpm and 4 °C and collection of the supernatant for purification.

The purification was performed by a Ni-NTA column that was pre-equilibrated with buffer B to facilitate loading of the cleared lysate. The impurities were washed off with buffer B having 10 and 20 mM imidazole. The bounded desired protein was eluted with a gradual increase in the concentration of imidazole (50−500 mM) in buffer B and was subjected to SDS-PAGE to confirm the purity of the protein. Eluted fractions showing the desired single band of the protein were subjected to dialysis against 100 mM NaCl and 25 mM Tris buffer pH 7.5 with five consecutive changes to obtain the refolded protein. The protein concentration was determined by a Jasco V-660 UV-Vis spectrophotometer at 280 nm using a molar extinction coefficient of 8730 M^{-1} cm^{-1}.[42]

5.6. Western Blotting. SDS-PAGE gel of the purified ectodomain G protein was transferred to the nitrocellulose membrane using the standard protocol. Blocking was done using 5% BSA in TBS at 25 °C for 2 h followed by three times washing. The membrane was incubated with 1:7000 dilution of the mouse anti-His monoclonal antibody in 1× TBS overnight at 4 °C. The membrane was washed thrice the next day to remove unbound antibodies. The bound antibody was incubated with 1:10 000 dilution of the HRP-conjugated anti-mouse immunoglobulin G (IgG) antibody in 1X TBS at 25 °C for 1 h followed by three times washing. Finally, the blot was developed with DAB and hydrogen peroxide (H$_2$O$_2$) or with luminal and H$_2$O$_2$ on an X-ray film.

5.7. Dynamic Light Scattering. Dynamic light scattering (DLS) was performed using a Malvern Zetasizer Nano-ZS instrument at the scattering angle of 173°, equipped with a He−Ne laser (λ = 632.8 nm). Before experiments were

performed, the sample was filtered through a 0.22 μm syringe filter. The protein concentration of 10 μM was used to perform the experiments, and at least three accumulations were taken. The hydrodynamic size was calculated using Origin 8 software.

5.8. Circular Dichroism Measurements. The secondary structure of the ectodomain G protein was determined by a Jasco spectropolarimeter (model J-1500) whose temperature was controlled by a Peltier device (MCB-100). The far-UV CD spectrum of the ectodomain G protein was recorded in the range of 250−200 nm using a cell of a path length 0.1 cm cuvette at 25 ± 0.1 °C. For sample preparation, 0.3 mg mL^{-1} protein concentration was used. Every spectrum scanning was carried out by taking an average of at least five accumulations. Experimental data of CD was converted into mean residue ellipticity $[\theta]_{\lambda}$ (degrees cm^2 dmol^{-1}) by the following relation

$$[\theta]_l = M_0[\theta]_l/10lc \tag{1}$$

where M_0 is the mean residue weight of the protein, $[\theta]_{\lambda}$ is the observed ellipticity in milli degrees at λ, c is the protein concentration in mg mL^{-1}, and l is the path length of the cell in centimeters. The baseline was always prepared with the respective buffers for avoiding the signal-to-noise ratio.

5.9. Measurements of Absorbance Spectra. The tertiary structure of the ectodomain G protein was determined by a Jasco V-660 UV-Vis spectrophotometer whose temperature was controlled with a Peltier device (ETCS-761). Every spectral measurement was carried out using a cell of a path length 1.0 cm cuvette in the wavelength range of 240−340 nm, and the temperature was maintained at 25 ± 0.1 °C. For sample preparation, 0.3 mg mL^{-1} protein concentration was used. Every measurement was done in triplicate, and their average was taken for data analysis.

5.10. Thermodynamic Protein Stability Measurements. For the thermal denaturant transition, the sample was heated at 1 °C min^{-1} in the range of 20−90 °C, and the change in absorbance was recorded as a function of temperature. The heating rate provides enough time to reach at equilibrium. The thermal denaturation of the ectodomain G protein was monitored, ε, at 280 nm. The raw sample data of absorbance was converted into molar extinction coefficient ($\Delta\varepsilon$) at a given wavelength. Thermal transition obtained from absorbance measurements was analyzed by Origin 8 software to determine the thermodynamic parameters like T_m and ΔH.

5.11. Fluorescence Spectroscopy. The intrinsic spectra of the ectodomain G protein at three different pH values were recorded by a Jasco spectrofluorometer (FP6200) at 25 ± 1 °C with a cell of a path length 1.0 cm quartz cuvette, and the temperature of the protein sample was controlled by a circulating water bath. We monitored the changes in the fluorescence intensity of the protein with different buffers taking the entrance and exit slit width of 5 nm. The emission spectra of the protein were observed in the wavelength range of 300−400, and the excitation wavelength was set at 280 nm. All of the spectra at a particular pH value were recorded in triplicate using the protein concentration of 0.3 mg mL^{-1}.

5.12. Isothermal Titration Calorimetry (ITC) Measurement. To analyze the thermodynamic parameters and binding affinity measurements, a VP-ITC calorimeter was used at 298 K (25 °C). The cell was injected for titration of the ectodomain G protein (10 μM) against the ligand (heparan sulfate, 200 μM concentration) in the ratio of 1:20 (protein:ligand). The ligand aliquots of 10 μL were loaded for each step in the interval of 300 s through the syringe along

with the buffer as a control. The experiment was carried out at physiological pH (7.5). The raw data obtained were normalized and accessed using the MicroCal Origin ITC software. The thermodynamic parameters like enthalpy change ($\Delta H°$), entropy change ($\Delta S°$), and the association constant (K_a) were obtained from the raw data using Origin 8.0. From the above thermodynamic parameters, the Gibbs free-energy change was calculated using the following equation

$$\Delta G° = -RT \ln K_a = \Delta H° - T\Delta S \qquad (2)$$

where R and T are the gas constant and temperature (in kelvins), respectively.

5.13. Microscale Thermophoresis (MST). To measure the biomolecular interaction, experiments based on changes in thermophoresis were performed by microscale thermophoresis in the Monolith NT.115 from NanoTemper Technologies.[43] Experiments were performed with MST power of 60%, LED power of 40%, and capillaries having a hydrophobic coating at standard conditions. In a typical label MST experiment, 20 μM ectodomain G protein was labeled with NT-647 (fluorescent dye) as per the manufacturer's instructions using the Monolith NT protein labeling kit. The fluorescence-labeled ectodomain G protein concentration was kept constant, and a serial dilution of the nonlabeled ligand, heparan sulfate, was prepared with Tris buffer. The highest concentration in the dilution series was chosen to be at least 20 times greater than the expected binding constant (K_d). Then, 10 μL of the nonlabeled ligand was mixed with 10 μL of the diluted fluorescent-labeled protein in the serial dilution experiment, and samples were loaded into Monolith NT.115 glass capillaries. As a result of titration, a gradual change had been observed in thermophoresis, which was plotted as ΔF_{norm} to find out the binding curve from which the value of the K_d was derived.

AUTHOR INFORMATION

Corresponding Author

Shama Parveen − *Centre for Interdisciplinary Research in Basic Sciences, Jamia Millia Islamia, New Delhi 110025, India;* orcid.org/0000-0001-5210-1442; Email: sparveen2@jmi.ac.in, shamp25@yahoo.com

Authors

Abu Hamza − *Centre for Interdisciplinary Research in Basic Sciences, Jamia Millia Islamia, New Delhi 110025, India*

Zoya Shafat − *Centre for Interdisciplinary Research in Basic Sciences, Jamia Millia Islamia, New Delhi 110025, India*

Zahoor Ahmad Parray − *Centre for Interdisciplinary Research in Basic Sciences, Jamia Millia Islamia, New Delhi 110025, India;* orcid.org/0000-0001-5998-7100

Malik Hisamuddin − *Interdisciplinary Biotechnology Unit, Aligarh Muslim University, Aligarh 202002, India*

Wajihul Hasan Khan − *Kusuma School of Biological Sciences, Indian Institute of Technology Delhi, New Delhi 110016, India*

Anwar Ahmed − *Centre of Excellence in Biotechnology Research, College of Science, King Saud University, Riyadh 11451, Saudi Arabia*

Fahad N. Almajhdi − *Department of Botany and Microbiology, College of Science, King Saud University, Riyadh 11451, Saudi Arabia; Centre of Excellence in Biotechnology Research, College of Science, King Saud University, Riyadh 11451, Saudi Arabia*

Mohamed A. Farrag − *Department of Botany and Microbiology, College of Science, King Saud University, Riyadh 11451, Saudi Arabia*

Arif Ahmed Mohammed − *Centre of Excellence in Biotechnology Research, College of Science, King Saud University, Riyadh 11451, Saudi Arabia*

Asimul Islam − *Centre for Interdisciplinary Research in Basic Sciences, Jamia Millia Islamia, New Delhi 110025, India;* orcid.org/0000-0001-9060-7970

Complete contact information is available at:
https://pubs.acs.org/10.1021/acsomega.1c00800

Notes

The authors declare no competing financial interest.

ACKNOWLEDGMENTS

REFERENCES

(1) Shi, T.; McAllister, D. A.; O'Brien, K. L.; Simoes, E. A.; Madhi, S. A.; Gessner, B. D.; Polack, F. P.; Balsells, E.; Acacio, S.; Aguayo, C.; Alassani, I.; et al. Articles Global, regional, and national disease burden estimates of acute lower respiratory infections due to respiratory syncytial virus in young children in 2015: a systematic review and modelling study. *Lancet* **2017**, *390*, 946−958.

(2) Nair, H.; Nokes, D. J.; Gessner, B. D.; Dherani, M.; Madhi, S. A.; Singleton, R. J.; O'Brien, K. L.; Roca, A.; Wright, P. F.; Bruce, N.; Chandran, A.; et al. Global burden of acute lower respiratory infections due to respiratory syncytial virus in young children: a systematic review and meta-analysis. *Lancet* **2010**, *375*, 1545−1555.

(3) Adams, M. J.; Lefkowitz, E. J.; King, A. M.; Harrach, B.; Harrison, R. L.; Knowles, N. J.; Kropinski, A. M.; Krupovic, M.; Kuhn, J. H.; Mushegian, A. R.; Nibert, M.; et al. Ratification vote on taxonomic proposals to the International Committee on Taxonomy of Viruses (2016). *Arch. Virol.* **2016**, *161*, 2921−2949.

(4) Higgins, D.; Trujillo, C.; Keech, C. Advances in RSV vaccine research and development - A global agenda. *Vaccine* **2016**, *34*, 2870−2875.

(5) Eshaghi, A.; Duvvuri, V. R.; Lai, R.; Nadarajah, J. T.; Li, A.; Patel, S. N.; Low, D. E.; Gubbay, J. B. Genetic variability of human respiratory syncytial virus a strains circulating in Ontario: A novel genotype with a 72 nucleotide G gene duplication. *PLoS One* **2012**, *7*, No. e32807.

(6) Roberts, S. R.; Lichtenstein, D.; Ball, L. A.; Wertz, G. W. The membrane-associated and secreted forms of the respiratory syncytial virus attachment glycoprotein G are synthesized from alternative initiation codons. *J. Virol.* **1994**, *68*, 4538−4546.

(7) Johnson, P. R.; Spriggs, M. K.; Olmsted, R. A.; Collins, P. L. The G glycoprotein of human respiratory syncytial viruses of subgroups A and B: extensive sequence divergence between antigenically related proteins. *Proc. Natl. Acad. Sci. U.S.A.* **1987**, *84*, 5625−5629.

(8) Cane, P. A.; Pringle, C. R. Respiratory syncytial virus heterogeneity during an epidemic: Analysis by limited nucleotide

sequencing (SH gene) and restriction mapping (N gene). *J. Gen. Virol.* **1991**, *72*, 349−357.

(9) Teng, M. N.; Collins, P. L. The Central Conserved Cystine Noose of the Attachment G Protein of Human Respiratory Syncytial Virus Is Not Required for Efficient Viral Infection In Vitro or In Vivo. *J. Virol.* **2002**, *76*, 6164−6171.

(10) Gorman, J. J.; Ferguson, B. L.; Speelman, D.; Mills, J. Determination of the disulfide bond arrangement of human respiratory syncytial virus attachment (G) protein by matrix-assisted laser desorption/ionization time-of-flight mass spectrometry. *Protein Sci.* **1997**, *6*, 1308−1315.

(11) Langedijk, J. P. M.; De Groot, B. L.; Berendsen, H. J. C.; Van Oirschot, J. T. Structural homology of the central conserved region of the attachment protein G of respiratory syncytial virus with the fourth subdomain of 55-kDa tumor necrosis factor receptor. *Virology* **1998**, *243*, 293−302.

(12) Feldman, S. A.; Hendry, R. M.; Beeler, J. A. Identification of a Linear Heparin Binding Domain for Human Respiratory Syncytial Virus Attachment Glycoprotein G. *J. Virol.* **1999**, *73*, 6610−6617.

(13) Johnson, S. M.; McNally, B. A.; Ioannidis, I.; Flano, E.; Teng, M. N.; Oomens, A. G.; Walsh, E. E.; Peeples, M. E. Respiratory syncytial virus uses CX3CR1 as a receptor on primary human airway epithelial cultures. *PLoS Pathog.* **2015**, *11*, No. e1005318.

(14) Escribano-Romero, E.; Rawling, J.; García-Barreno, B.; Melero, J. A. The Soluble Form of Human Respiratory Syncytial Virus Attachment Protein Differs from the Membrane-Bound Form in Its Oligomeric State but Is Still Capable of Binding to Cell Surface Proteoglycans. *J. Virol.* **2004**, *78*, 3524−3532.

(15) Valley-Omar, Z.; Muloiwa, R.; Hu, N. C.; Eley, B.; Hsiao, N. Y. Novel respiratory syncytial virus subtype ON1 among children, Cape Town, South Africa, 2012. *Emerging Infect. Dis.* **2013**, *19*, 668−670.

(16) Agoti, C. N.; Otieno, J. R.; Gitahi, C. W.; Cane, P. A.; James Nokes, D. Rapid spread and diversification of respiratory syncytial virus genotype ON1, Kenya. *Emerging Infect. Dis.* **2014**, *20*, 950−959.

(17) Malasao, R.; Okamoto, M.; Chaimongkol, N.; Imamura, T.; Tohma, K.; Dapat, I.; Dapat, C.; Suzuki, A.; Saito, M.; Saito, M.; Tamaki, R.; et al. Molecular Characterization of Human Respiratory Syncytial Virus in the Philippines, 2012-2013. *PLoS One* **2015**, *10*, No. e0142192.

(18) Takimoto, T.; Hurwitz, J. L.; Coleclough, C.; Prouser, C.; Krishnamurthy, S.; Zhan, X.; Boyd, K.; Scroggs, R. A.; Brown, B.; Nagai, Y.; Portner, A.; Slobod, K. S. Recombinant Sendai Virus Expressing the G Glycoprotein of Respiratory Syncytial Virus (RSV) Elicits Immune Protection against RSV. *J. Virol.* **2004**, *78*, 6043−6047.

(19) Sullender, W. Antigenic analysis of chimeric and truncated G proteins of respiratory syncytial virus. *Virology* **1995**, *209*, 70−79.

(20) Khan, W. H.; Srungaram, V. R.; Islam, A.; Beg, I.; Haider, M. S. H.; Ahmad, F.; Broor, S.; Parveen, S. Biophysical characterization of G protein ectodomain of group B human respiratory syncytial virus from *E. coli*. *Prep. Biochem. Biotechnol.* **2016**, *46*, 483−488.

(21) Dehaghani, S. A.; Babaeipour, V.; Mofid, M. R.; Divsalar, A.; Faraji, F. An efficient purification method for high recovery of Recombinant Human Granulocyte Colony Stimulating Factor from recombinant *E. coli*. *Int. J. Environ. Sci. Dev.* **2010**, *1*, 111−114.

(22) Yu, Z.; Reid, J. C.; Yang, Y. P. Utilizing dynamic light scattering as a process analytical technology for protein folding and aggregation monitoring in vaccine manufacturing. *J. Pharm. Sci.* **2013**, *102*, 4284−4290.

(23) Ferreira, J. C.; Rabeh, W. M. Biochemical and biophysical characterization of the main protease, 3-chymotrypsin-like protease (3CLpro) from the novel coronavirus SARS-CoV 2. *Sci. Rep.* **2020**, *10*, No. 22200.

(24) Tripp, R. A.; Jones, L. P.; Haynes, L. M.; Zheng, H.; Murphy, P. M.; Anderson, L. J. CX3C chemokine mimicry by respiratory syncytial virus G glycoprotein. *Nat. Immunol.* **2001**, *2*, 732−738.

(25) Hurwitz, J. L. Respiratory syncytial virus vaccine development. *Expert Rev. Vaccines* **2011**, *10*, 1415−1433.

(26) Harcourt, J.; Alvarez, R.; Jones, L. P.; Henderson, C.; Anderson, L. J.; Tripp, R. A Respiratory Syncytial Virus G Protein and G Protein CX3C Motif Adversely Affect CX3CR1 + T Cell Responses. *J. Immunol.* **2006**, *176*, 1600−1608.

(27) Boyoglu-Barnum, S.; Todd, S. O.; Meng, J.; Barnum, T. R.; Chirkova, T.; Haynes, L. M.; Jadhao, S. J.; Tripp, R. A.; Oomens, A. G.; Moore, M. L.; Anderson, L. J. Mutating the CX3C Motif in the G Protein Should Make a Live Respiratory Syncytial Virus Vaccine Safer and More Effective. *J. Virol.* **2017**, *91*, No. e02059-16.

(28) Chirkova, T.; Lin, S.; Oomens, A. G.; Gaston, K. A.; Boyoglu-Barnum, S.; Meng, J.; Stobart, C. C.; Cotton, C. U.; Hartert, T. V.; Moore, M. L.; Ziady, A. G.; Anderson, L. J. CX3CR1 is an important surface molecule for respiratory syncytial virus infection in human airway epithelial cells. *J. Gen. Virol.* **2015**, *96*, 2543−2556.

(29) Lee, H.-J.; Lee, J.-Y.; Park, M.-H.; Kim, J.-Y.; Chang, J. Monoclonal Antibody against G Glycoprotein Increases Respiratory Syncytial Virus Clearance In Vivo and Prevents Vaccine-Enhanced Diseases. *PLoS One* **2017**, *12*, No. e0169139.

(30) Jones, H. G.; Ritschel, T.; Pascual, G.; Brakenhoff, J. P.; Keogh, E.; Furmanova-Hollenstein, P.; Lanckacker, E.; Wadia, J. S.; Gilman, M. S.; Williamson, R. A.; Roymans, D.; van 't Wout, A. B.; Langedijk, J. P.; McLellan, J. S. Structural basis for recognition of the central conserved region of RSV G by neutralizing human antibodies. *PLoS Pathog.* **2018**, *14*, No. e1006935.

(31) Fuentes, S.; Klenow, L.; Golding, H.; Khurana, S. Preclinical evaluation of bacterially produced RSV-G protein vaccine: Strong protection against RSV challenge in cotton rat model. *Sci. Rep.* **2017**, *7*, No. 42428.

(32) Machado, V. B.; de Sá, J. M.; Prado, A. K. M.; de Toledo, K. A.; Regasini, L. O.; de Souza, F. P.; Caruso, Í.P.; Fossey, M. A. Biophysical and flavonoid-binding studies of the G protein ectodomain of group A human respiratory syncytial virus. *Heliyon* **2019**, *5*, No. e01394.

(33) Martin-Gallardo, A.; Fleischer, E.; Doyle, S. A.; Arumugham, R.; Collins, P. L.; Hildreth, S. W.; Paradiso, P. R. Expression of the G glycoprotein gene of human respiratory syncytial virus in Salmonella typhimurium. *J. Gen. Virol.* **1993**, *74*, 453−458.

(34) Opekarová, M.; Tanner, W. Specific lipid requirements of membrane proteins - A putative bottleneck in heterologous expression. *Biochim. Biophys. Acta, Biomembr.* **2003**, *1610*, 11−22.

(35) Miroux, B.; Walker, J. E. Over-production of proteins in Escherichia coli_ mutant hosts that allow synthesis of some membrane proteins and globular proteins at high levels. *J. Mol. Biol.* **1996**, *260*, 289−298.

(36) Lundstrom, K. Structural genomics for membrane proteins. *Cell. Mol. Life Sci.* **2006**, *63*, 2597−2607.

(37) Battles, M. B.; McLellan, J. S. Respiratory syncytial virus entry and how to block it. *Nat. Rev. Microbiol.* **2019**, *17*, 233−245.

(38) Parray, Z. A.; Ahmad, F.; Hassan, M. I.; Hasan, I.; Islam, A. Effects of Ethylene Glycol on the Structure and Stability of Myoglobin Using Spectroscopic, Interaction, and in Silico Approaches: Monomer Is Different from Those of Its Polymers. *ACS Omega* **2020**, *5*, 13840−13850.

(39) Ahanger, I. A.; Parray, Z. A.; Nasreen, K.; Ahmad, F.; Hassan, M. I.; Islam, A.; Sharma, A. Heparin Accelerates the Protein Aggregation via the Downhill Polymerization Mechanism: Multi-Spectroscopic Studies to Delineate the Implications on Proteino-pathies. *ACS Omega* **2021**, *6*, 2328−2339.

(40) Hileman, R. E.; Fromm, J. R.; Weiler, J. M.; Linhardt, R. J. Glycosaminoglycan-protein interactions: Definition of consensus sites in glycosaminoglycan binding proteins. *BioEssays* **1998**, *20*, 156−167.

(41) Thammawat, S.; Sadlon, T. A.; Hallsworth, P. G.; Gordon, D. L. Role of Cellular Glycosaminoglycans and Charged Regions of Viral G Protein in Human Metapneumovirus Infection. *J. Virol.* **2008**, *82*, 11767−11774.

(42) Pace, C. N.; Vajdos, F.; Fee, L.; Grimsley, G.; Gray, T. How to measure and predict the molar absorption coefficient of a protein. *Protein Sci.* **1995**, *4*, 2411−2423.

(43) Wienken, C. J.; Baaske, P.; Rothbauer, U.; Braun, D.; Duhr, S. Protein-binding assays in biological liquids using microscale thermophoresis. *Nat. Commun.* **2010**, *1*, No. 100.